Improved extrapolation of steady turbulent aerodynamics using a non-linear POD-based reduced order model

R. Zimmermann
ralf.zimmermann@tu-bs.de
Institute Computational Mathematics
TU Braunschweig
Germany

S. Görtz
Institute of Aerodynamics and Flow Technology
German Aerospace Center (DLR)
Germany

ABSTRACT

A reduced-order modelling (ROM) approach for predicting steady, turbulent aerodynamic flows based on computational fluid dynamics (CFD) and proper orthogonal decomposition (POD) is presented. Model-order reduction is achieved by parameter space sampling, solution space representation via POD and restriction of a CFD solver to the POD subspace. Solving the governing equations of fluid dynamics is replaced by solving a non-linear least-squares optimisation problem. The method will be referred to as LSQ-ROM method. Two approaches of extracting POD basis information from CFD snapshot data are discussed: POD of the full state vector (global POD) and POD of each of the partial states separately (variable-by-variable POD). The method at hand is demonstrated for a 2D aerofoil (NACA 64A010) as well as for a complete industrial aircraft configuration (NASA Common Research Model) in the transonic flow regime by computing ROMs of the compressible Reynolds-averaged Navier-Stokes equations, pursuing both the global and the variable-by-variable POD approach. The LSQ-ROM approach is tried for extrapolatory flow conditions. Results are juxtaposed with those obtained by POD-based extrapolation using Kriging and the radial basis functions spline method. As a reference, the full-order CFD solutions are considered. For the industrial aircraft configuration, the cost of computing the reduced-order solution is shown to be two orders of magnitude lower than that of computing the reference CFD solution.

Paper No. 3672. Manuscript received 19 November 2010,
revised version received 23 December 2011, accepted 17 January 2012.

https://doi.org/10.1017/S0001924000007491 Published online by Cambridge University Press

NOMENCLATURE

$\mathbf{a} \in \mathbb{R}^{\tilde{m}}$	vector of POD coefficients
$\mathbf{A} \in \mathbb{R}^{n_t}$	mean flow state vector of the first $\tilde{m}$ POD eigenmodes
$C_L, C_D \in \mathbb{R}$	lift and drag coefficients
$C_p \in \mathbb{R}$	pressure coefficient
$d \in \mathbb{N}$	number of model parameters
$E \in \mathbb{R}$	total energy
f_i	ith flow variable, e.g. $f_1 = \rho$
$\mathbf{I} \in \mathbb{R}^{n \times n}$	identity matrix
$\mathrm{Ma} \in \mathbb{R}$	Mach number
$m \in \mathbb{N}$	number of flow solution snapshots
$\tilde{m} \in \mathbb{N}$	dimension of POD subspace (global POD)
$\tilde{M} \in \mathbb{N}$	dimension of POD subspace (variable-by-variable POD)
$n \in \mathbb{N}$	number of grid points
$n_t = nv \in \mathbb{N}$	total dimension of discretised flow problem
$\mathbf{p} \in \mathbb{R}^d$	vector of model parameters
$\mathrm{res} : \mathbb{R}^{n_t} \rightarrow \mathbb{R}^{n_t}$	discretised flux residual
$\mathrm{RIC}(\tilde{m})$	relative information content of the first $\tilde{m}$ POD eigenmodes
$r_j \in \mathbb{R}$	RIC of the jth POD mode
$(u_x, u_y, u_z) \in \mathbb{R}^3$	flow velocity vector
$U^j \in \mathbb{R}^{n_t}$	jth POD mode
$V^j \in \mathbb{R}^m$	jth eigenvector of $\mathbf{Y}^{\mathrm{T}}\Omega\mathbf{Y}$
$v \in \mathbb{N}$	number of flow variables
$\mathbf{W} \in \mathbb{R}^{n_t}$	flow solution state vector
$\mathbf{Y} \in \mathbb{R}^{n_t \times m}$	snapshot matrix
$x, y, z \in \mathbb{R}$	cartesian spatial co-ordinates
$\alpha[^\circ]$	angle-of-attack
$\lambda_j \in \mathbb{R}$	jth eigenvalue of $\mathbf{Y}^{\mathrm{T}}\Omega\mathbf{Y}$
$\mu_t \in \mathbb{R}$	eddy viscosity
$\nu \in \mathbb{R}$	Spallart-Allmaras viscosity
$\rho \in \mathbb{R}$	density
$\Omega \in \mathbb{R}^{n_t \times n_t}$	diagonal matrix of grid cell volumes
$\langle \cdot, \cdot \rangle_{L_2}$	L_2 scalar product
$\|\cdot\|_{L_2} = \sqrt{\langle \cdot, \cdot \rangle_{L_2}}$	L_2 norm

1.0 INTRODUCTION

From an aerodynamic point of view, an aircraft is defined by comprehensive data sets regarding performance, loads and handling qualities. This data, which needs to be determined at a given timescale and cost for every possible flight condition and aircraft configuration, is used to design the structure of the aircraft and the flight control system. Currently, this data is obtained mainly from costly wind tunnel tests or using hand-book methods. The use of higher-fidelity and thus more accurate but also more time consuming CFD (computational fluid dynamics) methods has been, up to now, impossible due to the large number of load cases that need to be evaluated to achieve aircraft certification. Only a subset of the required data can be computed with high-fidelity CFD at present. The 'brute-force' approach of computing all relevant data with high-fidelity CFD is not feasible at present and methods for reducing the computational cost are sought after.

https://doi.org/10.1017/S0001924000007491 Published online by Cambridge University Press

CFD simulations are also of limited use in various multi-disciplinary settings that require the aerodynamics to be simulated repeatedly, including fluid-structure interaction problems, design and optimisation, probabilistic applications, and real-time applications such as flow control. This situation will improve with sustained advances in computing power, but at the same time, it is likely that even greater fidelity in terms of turbulence modeling or grid size will be desired as more detailed flow features and geometrical complexities are addressed in CFD simulations. Thus, there is a fundamental gap between the CFD fidelity used to simulate an aircraft at a single flow condition and that practical for multi-disciplinary analysis and aircraft design. This suggests that computed CFD data need to be distilled into lower-order models to replace the CFD code in, for example, multi-disciplinary simulations. The intent in constructing such reduced-order models (ROMs) is to provide quantitatively accurate descriptions of the aerodynamics with fewer degrees of freedom and thus much lower evaluation time than the original CFD model[1-3].

As an initial step towards these long-term goals, the objective of this paper is to demonstrate the ability of proper orthogonal decomposition (POD), in combination with high-fidelity CFD, to produce reduced-order models (ROMs) for three-dimensional, turbulent, compressible flows that can be used to predict the aerodynamic loads acting on full aircraft configurations at reduced computational cost. The present paper can be considered a follow up to[4,5], where the authors adapted the reduced-order modelling approach of LeGresley and Alonso[6] for predicting steady aerodynamic flows and loads data. The method can be summarised as follows: After sampling a model parameter space of interest by computing so-called 'snapshot' flow solutions with a CFD solver at a finite number of model parameter combinations (e.g. combinations of Mach number and angle-of-attack), POD is performed to obtain a (possibly reduced) orthogonal representation of the space spanned by these snapshots. To predict flow solutions at unsampled locations in the model parameter space, the CFD flow solver is restricted to the POD subspace and a non-linear least-squares optimisation problem is solved. The method will be referred to as POD-subspace restricted least-squares method (LSQ-ROM); our CFD solver of choice is the DLR TAU code[7-9]. The work presented herein goes beyond that presented in Ref. 4 in the following way:

- A comparison of global POD and variable-by-variable POD is presented. The first approach relies on a POD basis for all flow variables simultaneously, while a separate POD basis is computed for each flow variable in the latter one.
- It is proved that for POD interpolation schemes using radial basis functions (RBFs, see Ref. 10, §2.3 for a short introduction) the global and variable-by-variable POD approaches coincide.
- For the first time, a LSQ-ROM based on the compressible Reynolds-averaged Navier-Stokes equations (RANS) is applied to a large industrial aircraft configuration at transonic flow conditions.

Recently, other promising approaches for non-linear model reduction have been suggested, amongst them the discrete empirical interpolation method (DEIM)[11] and the missing point estimation (MPE)[12]. Both of these approaches are based on a classical Galerkin projection of the governing equations onto the POD-subspace. In order to achieve effective model order reduction for non-linear problems, a mask matrix is applied to filter out the most significant residuals from the projected residual equations. So far, both methods have never been applied in an industrial context, one reason being, presumably, that they require extensive modifications of the flow solver source code. The method presented here, however, has the advantage that it is relatively easy to implement using an existing industrial CFD code, a fact not to be underestimated.

https://doi.org/10.1017/S0001924000007491 Published online by Cambridge University Press

We start out demonstrating the LSQ-ROM method by computing reduced-order solutions to the compressible RANS equations for the NACA 64A010 aerofoil based on a set of snapshots in the transonic flow regime, where shocks, or, mathematically speaking, discontinuities occur. Results of the global LSQ-ROM and the variable-by-variable LSQ-ROM are compared with those obtained by POD-based interpolation[13] using Kriging[14,15] as well as the thin plate spline RBF method[10], and with a reference CFD solution.

Subsequently, we use the method to derive a ROM for the transonic turbulent flow around the NASA common research model[16], a wide-body commercial passenger aircraft configuration, comparing the results again to those obtained by POD-based extrapolation and full-order CFD.

In both cases, flow solutions are predicted at extrapolatory flow conditions with respect to the snapshot data set. Accuracy is quantified by comparing surface pressure distributions and integrated aerodynamic coefficient values. The order reduction and computational performance of the reduced-order model is also quantified relative to the full order simulation. The capability of the method in the (less challenging) case of interpolation was demonstrated in Ref. 19.

2.0 THEORETICAL BACKGROUND

Considering the Navier-Stokes equations (NSEs), spatially discretised on a grid of size n for some aerodynamic configuration, let v be the corresponding number of primitive mean flow variables plus the number of primitive variables associated with the turbulence model. The primitive mean flow variables are the density, ρ, the velocity components in all spatial directions, u_x, u_y, u_z, and the total energy, E. The number of primitive turbulence variables depends on the chosen turbulence model. Let $n_t = nv$ denote the total length of the discretised flow solution vectors. The system of ordinary differential equations in pseudo-time to be solved can be written as

$$\frac{\mathrm{d}}{\mathrm{d}t}\mathbf{W} + \Omega^{-1}\,\mathrm{res}(\mathbf{W}) = 0 \in \mathbb{R}^{n_t}, \qquad \ldots (1)$$

where $\mathbf{W} \in \mathbb{R}^{n_t}$ is the vector of primitive variables, $\mathrm{res}(\mathbf{W}) \in \mathbb{R}^{n_t}$ is the vector of flux residuals corresponding to the state solution $\mathbf{W}$ and $\Omega \in \mathbb{R}^{n_t \times n_t}$ is a diagonal matrix with v blocks, each containing the volumes (vol_1, ..., vol_n) of the corresponding grid cells on the diagonal. Denoting by $W_{k,i}$ the value of flow variable k corresponding to grid cell i and by $\mathrm{res}_{k,i}(\mathbf{W})$ the flux residual of flow variable k in grid cell i, Equation (1) may be written in cell-wise form as

$$\forall k = 1,\ldots,v \quad \forall i = 1,\ldots,n: \quad \frac{\mathrm{d}}{\mathrm{d}t}W_{k,i} + \frac{1}{vol_i}\mathrm{res}_{k,i}(\mathbf{W}) = 0, \qquad \ldots (2)$$

see §5, Equation (5.3) in Ref. 17 for an equivalent formulation in conservative variables. The steady state is achieved if the time derivative drops out in Equations (1) and (2), or, equivalently, if the CFD flux residual vanishes

$$0 = \Omega^{-1}\mathrm{res}(\mathbf{W}) \in \mathbb{R}^{n_t} \qquad \ldots (3)$$

Remark: All flow solutions employed in this study were computed with the DLR TAU code[7-9]. For the Spalart-Allmaras one-equation turbulence model the TAU residual vector includes the

https://doi.org/10.1017/S0001924000007491 Published online by Cambridge University Press

density residual, the velocity residuals, the energy residual, and the SA-viscosity residual,

$$\mathrm{res}(\mathbf{W}) = (\mathrm{res}(\rho), \mathrm{res}(u_x), \mathrm{res}(u_y), \mathrm{res}(u_z), \mathrm{res}(E), \mathrm{res}(\nu))^T \quad \ldots (4)$$

while the flow solution vector includes the density, the velocities, the pressure, the SA-viscosity and the eddy-viscosity, i.e.

$$\mathbf{W} = (\rho, u_x, u_y, u_z, p, \nu, \mu_t)^T \quad \ldots (5)$$

The ROM method presented in the following is by no means restricted to flow state vectors given in primitive variables, but applies also to state vectors in conservative variables or even different governing PDE problems.

2.1 Reduced-order modelling via proper orthogonal decomposition

A short review of POD-based ROM approaches in finite dimensional vector spaces is given in Refs 4, 18 and 19 for a comprehensive introduction, see Ref. 20 and references therein. For the reader's convenience we will briefly review the essentials.

Let $p_1, \ldots, p_d$ be the independent flow parameters considered for building the reduced-order model. Suppose that we are given m steady CFD flow solution snapshots $\mathbf{W}^i := \mathbf{W}(\mathbf{p}^i) \in \mathbb{R}^{n_t}$, where $\boldsymbol{p}^i = (p_1^i, \ldots, p_d^i) \in \mathbb{R}^d$ denotes the ith combination of model parameters, e.g. $\boldsymbol{p}^i = (p_1^i, p_2^i) = (\mathrm{Ma}_i, \alpha_i)$ for a problem with $d = 2$ parameters. The corresponding centred snapshot matrix is defined by:

$$\mathbf{Y} = (\tilde{\mathbf{W}}^1, \ldots, \tilde{\mathbf{W}}^m) \in \mathbb{R}^{n_t \times m} \quad \ldots (6)$$

where $\tilde{\mathbf{W}}^i = \mathbf{W}^i - \mathbf{A}$ are the centred snapshots with $\mathbf{A} = \frac{1}{m}\sum_{j=1}^{m} \mathbf{W}^j$ being the average of all snapshots. With respect to the discrete L_2 scalar product $\langle \mathbf{W}_a, \mathbf{W}_b \rangle_{L_2} = \mathbf{W}_a^T \Omega \mathbf{W}_b$ associated with the computational domain, the orthonormal basis $\{\mathbf{U}^1, \ldots, \mathbf{U}^{m-1}\}$ of POD eigenmodes satisfying

$$\mathrm{span}\{\mathbf{U}^1, \ldots, \mathbf{U}^{m-1}\} = \mathrm{span}\{\tilde{\mathbf{W}}^1, \ldots, \tilde{\mathbf{W}}^m\} \quad \ldots (7)$$

is given by

$$\mathbf{U}^j = (\sqrt{\lambda_j})^{-1} \mathbf{Y} \mathbf{V}^j \in \mathbb{R}^{n_t}, \quad j = 1, \ldots, m-1, \quad \ldots (8)$$

where the vectors $\mathbf{V}^j \in \mathbb{R}^m$ are the normalised eigenvectors of the $m \times m$-dimensional eigenvalue problem

$$(\mathbf{Y}^T \Omega \mathbf{Y}) \mathbf{V}^j = \lambda_j \mathbf{V}^j, \; j = 1, \ldots, m \quad \ldots (9)$$

Since the centred snapshots are linearly dependent, a maximum of $m - 1$ POD modes is sufficient for a perfect reconstruction of the snapshots. The ordering of the eigenvectors is with respect to the size of the corresponding eigenvalues $\lambda_1 > \lambda_2 > \ldots > \lambda_m$, thus $\mathbf{V}^1$ and consequently $\mathbf{U}^1$ corresponds to the largest eigenvalue λ_1 and so forth.

The relative information content of the jth mode is defined as the ratio $r_j = \lambda_j / (\sum_{i=1}^{m} \lambda_i)$ and the relative information content (RIC) of the first $\tilde{m} \leq m - 1$ basis modes is thus given by:

https://doi.org/10.1017/S0001924000007491 Published online by Cambridge University Press

$$\mathrm{RIC}(\tilde{m}) = \sum_{i=1}^{\tilde{m}} r_i. \qquad \ldots (10)$$

The space spanned by the first $\tilde{m} \leq m - 1$ POD basis modes is the best order-$\tilde{m}$-representation of the initial snapshot space with respect to the underlying scalar product. After the POD, an approximate flow solution can be constructed based on coefficient vectors $\mathbf{a} = (a_1, ..., a_{\tilde{m}}) \in \mathbb{R}^{\tilde{m}}$ as follows:

$$\mathbf{W}(\mathbf{a}) = \mathbf{A} + \left(\mathbf{U}^1, ..., \mathbf{U}^{\tilde{m}} \right) \mathbf{a} = \mathbf{A} + \sum_{j=1}^{\tilde{m}} a_j \, \mathbf{U}^j. \qquad \ldots (11)$$

The (possibly) reduced representation of the ith snapshot solution is given by

$$\mathbf{W}^i(\mathbf{a}) = A + \sum_{j=1}^{\tilde{m}} a_j^i \, \mathbf{U}^j, \text{with coefficients } a_j^i = \langle \mathbf{W}^i, \mathbf{U}^j \rangle_{L_2} = \frac{1}{\sqrt{\lambda_j}} \mathbf{W}^{iT} \Omega \, \mathbf{Y} \mathbf{V} = \sqrt{\lambda_j} \, \mathbf{V}_i^j. \qquad \ldots (12)$$

According to Equation (11), the computation of an approximate flow solution at an untried parameter condition $\mathbf{p}^*$ via POD is reduced to computing the POD coefficient vector $\mathbf{a}(\mathbf{p}^*) := \mathbf{a}^* = (\mathbf{a}^*_1, ..., \mathbf{a}^*_{\tilde{m}})$. For the results presented in this paper, two approaches for determining POD coefficients were pursued, the first being the so-called POD-based interpolation method[13]. Here, for each $j = 1, ..., \tilde{m}$, the scalar-valued coefficient a^*_j is obtained by interpolating the sample values $a^1_j = a_j(p^1), ..., a^m_j = a_j(p^m)$ given by Equation (12). The choice of an appropriate interpolation method is problem dependent. In this work, Kriging[15,21] and the thin plate spline method (TPS)[10] were used for multi-dimensional scattered-data interpolation.

While the POD-based interpolation method outlined above is entirely mathematics-based, the second approach, proposed in Ref. 6, takes flow physics into account; the coefficients of the reduced solution are determined by minimising the associated CFD flux residual, which is evaluated using a full-order CFD solver. Therefore, the order-n_t equation system Equation (3) is replaced by the unconstrained non-linear least squares optimisation problem

$$\min_{\mathbf{a}=(a_1,...,a_{\tilde{m}})} \left\| \Omega^{-1} \mathrm{res}(\mathbf{W}(\mathbf{a})) \right\|^2_{L_2} = \sum_{k=1}^{v} \sum_{i=1}^{n} \frac{1}{vol_i} \left(\mathrm{res}_{k,i}(\mathbf{W}(\mathbf{a})) \right)^2. \qquad \ldots (13)$$

Of all flow solution vectors that allow for a representation of the form (Equation (11)) , i.e., all flow solution vectors contained in the POD subspace, the solution to Equation (13) is closest to a converged CFD solution for the given parameter combination in a least-squares average sense. For solving Equation (13), the gradient-based Levenberg-Marquardt algorithm (Ref. 22, Alg 3.34), a damped Gauß-Newton method, is applied. As an initial step, the Jacobian of the flux residual with respect to the POD coefficients is computed via finite differences approximations. In order to keep the computational effort as low as possible, subsequently, Broyden updates[22], of the Jacobian are used throughout the optimisation process. In order to allow for the same impact of all residual variables on the optimisation problem (Equation (13)) regardless of their scale, for each flow variable, the residuals are normalised by the corresponding mean value of the residuals of the initial solution.

In contrast to POD-based interpolation, the sampled POD-coefficients of the snapshots according to Equation (12) are not used in determining the optimised coefficients. Thus, the least-squares ROM approach is *per se* better suited for extrapolation.

https://doi.org/10.1017/S0001924000007491 Published online by Cambridge University Press

Mnemonic: All POD-based methods boil down to estimating POD coefficients rather than solution vector entries. The approximate solution is constructed based entirely on the information contained in the initial snapshot set.

2.2 Global POD *vs* variable-by-variable POD

In this work, global POD refers to POD of the full state vector, featuring the complete flow-field data, e.g. $\mathbf{W} = (\rho, u_x, u_y, u_z, p, \nu, \mu_t)^T$. Therefore, the requirements on global POD basis modes are the following:

- they have to account for variables of different magnitude and units,
- they have to capture the main features of the solution for each flow variable simultaneously,
- any linear combination of modes should result in a physically admissible solution.

In order to obtained a balanced influence of all variables, a non-dimensionalisation of the flow data was proposed in Refs 4 and 5. However, as recent work[19] suggests that a pressure dominated POD is beneficial for obtaining good surface pressure approximations, we refrained from using non-dimensional data in this work.

In the context of reduced-order modelling of flow solutions, both the density and the pressure occur as primitive variables and both quantities have to be to be strictly positive. Note that in contrast to the density values themselves, their fluctuations around the mean value may very well feature negative values. Hence, centering the snapshots by subtracting the snapshot average as outlined in Section 2.1 can be considered a mandatory step towards mapping the data onto a suitable vector space, see Ref 19, §2.3 for a detailed discussion.

For the variable-by-variable POD approach, the snapshot vectors $\{\mathbf{W}^1, ...,\mathbf{W}^m\}$ are considered as partitioned into sub-blocks, one for each primitive flow variable $f_1, ..., f_v$, i.e.

$$\mathbf{W}^i = \begin{pmatrix} \mathbf{W}^i_{f_1} \\ \vdots \\ \mathbf{W}^i_{f_v} \end{pmatrix} \in \mathbb{R}^{n_t} \text{ with } \mathbf{W}^i_{f_k} = \left(W^i_{f_k,1},...,W^i_{f_k,n}\right)^T \in \mathbb{R}^n \text{ for } k = 1,...,v. \quad \ldots (14)$$

A POD of the data set $\{\mathbf{W}^1_{fk}, ...,\mathbf{W}^m_{fk}\}$ associated to flow variable f_k results in a (possibly reduced) set of POD eigenmodes $\{\mathbf{U}^1_{fk}, ...,\mathbf{U}^{\tilde{m}_k}_{fk}\}$, where the reduced-order $\tilde{m}_k \leq m - 1$ is determined based on the RIC with respect to the flow variable at hand. Note that the reduced dimensions do not have to coincide, i.e. $\tilde{m}_k \neq \tilde{m}_l$ is allowed for $f_k \neq f_l$.

For the variable-by-variable POD approach, the POD coefficient vector is of the form

$$\mathbf{a} = \left(a_{f_1,1},...,a_{f_1,\tilde{m}_1},...,a_{f_v,1},...,a_{f_v,\tilde{m}_v}\right) \in \mathbb{R}^{\tilde{M}}, \text{ where } \tilde{M} = \sum_{k=1}^{v} \tilde{m}_k, \quad \ldots (15)$$

and the corresponding approximate flow solution is constructed as:

$$\mathbf{W}(\mathbf{a}) = A + \begin{pmatrix} \sum_{l=1}^{\tilde{m}_1} a_{f_1,l}\ \mathbf{U}^l_{f_1} \\ \vdots \\ \sum_{l=1}^{\tilde{m}_v} a_{f_v,l}\ \mathbf{U}^l_{f_v} \end{pmatrix} \in \mathbb{R}^{n_t}, \quad \ldots (16)$$

https://doi.org/10.1017/S0001924000007491 Published online by Cambridge University Press

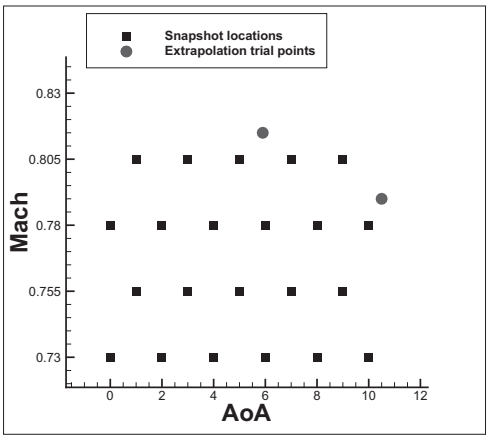

Figure 1. Snapshot sample locations and reduced-order model trial points in the Mach-α space.

compare to Equation 12. Although each subpart of the coefficient vector **a** affects only the associated subpart of the flow solution vector **W**, the residual res(**W**(**a**)) and therefore the optimisation problem (Equation 13) depends on all coefficients.

While only one eigenvalue decomposition of a matrix of size $m \times m$ is due for the global POD approach, **v** matrix decompositions of the same precise order have to be performed for the variable-by-variable ansatz. The order of the least-squares optimisation problem (Equation 13) replacing the governing Equation 3 is $\tilde{m} \leq m$ and $\tilde{M} = \sum_{k=1}^{v} \tilde{m}_k \leq vm$, respectively.

The memory requirements for storing the POD modes are the same for both approaches. The Jacobian to be constructed as part of the optimisation with respect to global modes reads $D(\text{res} \circ \mathbf{W})(\mathbf{a}) \in \mathbb{R}^{n_t \times \tilde{m}}$. With respect to variable-by-variable modes, it reads $D(\text{res} \circ \mathbf{W})(\mathbf{a}) \in \mathbb{R}^{n_t \times \tilde{M}}$ and therefore requires, as a rule of thumb, storing about v times more columns.

Although more costly, the variable-by-variable approach allows for a more detailed exploitation of the information contained in the snapshots, with the space of representable solutions being enlarged. Thus, fine tuning of the POD coefficients and thus a smaller flux residual of the corresponding approximate solution is rendered possible. In addition, the problem of data scaling is avoided. In practical applications, these advantages have to be contrasted with the higher computational expenses.

2.3 Some fundamental facts about POD-based interpolation via RBFs

1. Entry-by-entry interpolation of the snapshot vectors and interpolation of the basis coefficients when considering the snapshot vectors themselves as a basis lead to the same results when applying radial basis function interpolation. Provided that the maximum number of POD modes $\tilde{m} = m - 1$ is retained in the POD basis, then RBF interpolation of POD coefficients with respect to global POD modes and RBF interpolation of POD coefficients with respect to variable-by-variable POD modes again lead to the same result. It is understood that with respect to the numerical effort, interpolating basis coefficients is is much more efficient than entry-by-entry interpolation of vectors with, say, several million entries.
2. Performing RBF interpolation on vector-valued flow field data and subsequently computing the corresponding lift, drag and moment coefficients leads to exactly the same result as

https://doi.org/10.1017/S0001924000007491 Published online by Cambridge University Press

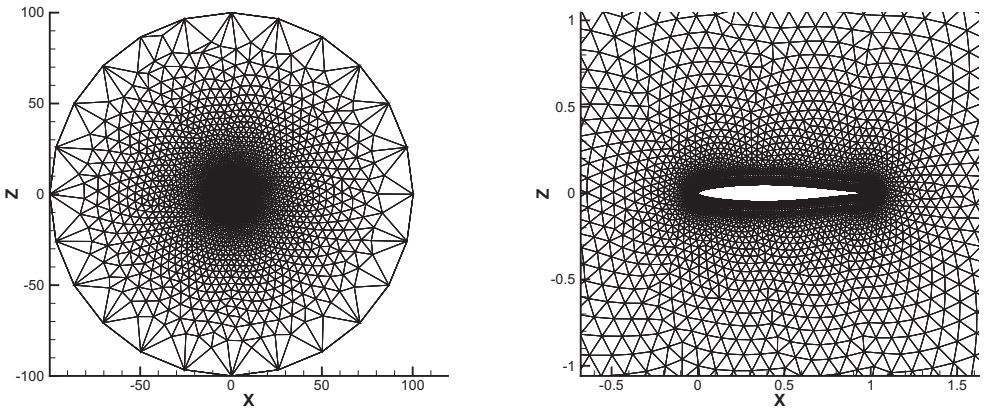

Figure 2. Computational grid for the NACA 64A010 aerofoil with 10,727 grid points.
Left: farfield grid. Right: detailed view of volume grid around the aerofoil.

performing RBF interpolation on the scalar integrated coefficients only, without knowing any surface distribution.

These facts are stated precisely and proved in the Appendix.

3.0 RESULTS

First demonstrations of the POD-subspace restricted least-squares (LSQ-ROM) method for modelling steady flow at transonic flow conditions based on the compressible Euler equations and steady subsonic flow based on the Navier-Stokes equations were presented in Refs 4 and 5. Here, we present applications to fully turbulent, transonic flows in both two and three dimensions at extrapolatory flow conditions.

3.1 Navier-Stokes LSQ-ROM for transonic flow around the NACA 64A010 aerofoil

In this section, we present a reduced-order model of the compressible Navier-Stokes equations for the NACA 64A010 aerofoil. The model with two independent parameters, Mach number, *Ma*, and angle-of-attack, α, is built based on snapshots in the transonic flow regime. For computing snapshot flow solutions, the unstructured DLR RANS solver TAU[7-9] is applied using the Spalart-Allmaras one-equation turbulence model, see §7.2.1 in Ref. 17. The Reynolds number is fixed at a value of 7,500,000. The POD basis is constructed relying on 22 snapshots at pairs of $(\alpha,\mathrm{Ma}) \in [0°, 10°] \times [0{\cdot}73, 0{\cdot}805]$. The precise snapshot sample locations are plotted in Fig. 1. The unstructured computational grid used for computing the snapshots with TAU features 10,727 grid points and is shown in Fig. 2.

A global POD of the snapshot data results in an orthogonal representation, where the global modes are represented by vectors of dimension $n_t = vn = 6 \cdot 10{,}727 = 128{,}724$. To capture the complete information content, the maximum number of 21 POD modes is kept in the POD basis. Pursuing the variable-by-variable POD approach, we obtain POD sub-bases for density, *x*-

https://doi.org/10.1017/S0001924000007491 Published online by Cambridge University Press

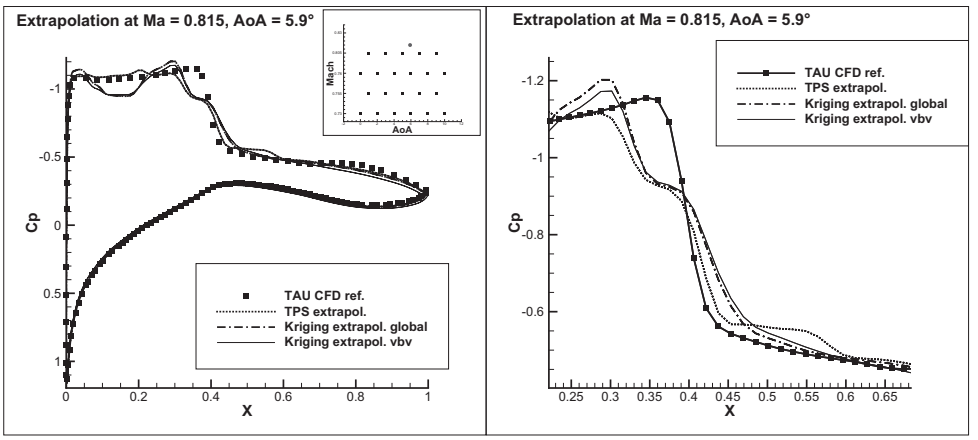

Figure 3. Comparison of the surface C_p-distributions for NACA 64A010 aerofoil approximated via TPS extrapolation and global and variable-by-variable Kriging extrapolation with the converged reference TAU CFD solution at Ma = 0·815 and α = 5·9°. Right: detailed view of the shock region.

velocity, z-velocity, pressure, the SA-viscosity and the eddy-viscosity, each consisting of 21 POD modes that capture the complete relative information content, leading to a total of $6 \cdot 21 = 126$ mode vectors of size n = 10,727. Note that the mean flow vector is the same for both approaches and is a constant vector that is not subject to any estimation/optimisation procedure.

Hence, according to Equation (13), the initial flow problem of order n_t = 10,727 is reduced to an order-21 optimisation problem for global POD while it is reduced to an order-126 optimisation problem for variable by-variable POD.

Reduced-order flow predictions were computed at trial conditions of (α, Ma) = (5·9°, 0·815) and (α, Ma) = (10·5°, 0·79). Note that both points lie outside of the convex hull of the snapshot data, see Fig. 1. Hence, they define extrapolatory flow conditions with respect to the sample snapshot set. The TAU reference solution at (α, Ma) = (5·9°, 0·815) converged after 2,137 pseudo-time steps to a normalised (density) residual of 10^{-7}, at (α, Ma) = (10·5°, 0·79) it took 3,927 iterations to converge to the same level.

In the following, results of the global and the variable-by-variable LSQ-ROM are juxtaposed with those obtained by POD-based extrapolation using Kriging and the RBF approach with thin-plate spline (TPS) correlation. The TPS-extrapolated solution was used as a starting point for the LSQ-ROM optimisation in all cases.

In addition to the option of employing global *vs* variable-by-variable POD bases, the LSQ-ROM residual optimisation procedure (Equation 13) was conducted either with respect to all flow variables (AFV-Res) or with respect to the mean flow variables (MFV-Res) only. More precisely, for the option 'AFV-Res', all sub-blocks of the residual vector as given in Equation (4) were considered in Equation (13), while for the option 'MFVRes', the residuals corresponding to the turbulent SA-viscosity, res(ν), were excluded. A larger number of options in setting up the LSQ-ROM process was introduced and discussed in Ref. 19.

3.1.1 Extrapolation at (Ma = 0·815, α = 5·9°)

Figures 3 and 4 display the surface C_p-distributions obtained via the various methods at the trial condition (Ma = 0·815, α = 5·9°). The results of POD-based extrapolation, shown in Fig. 3, all

https://doi.org/10.1017/S0001924000007491 Published online by Cambridge University Press

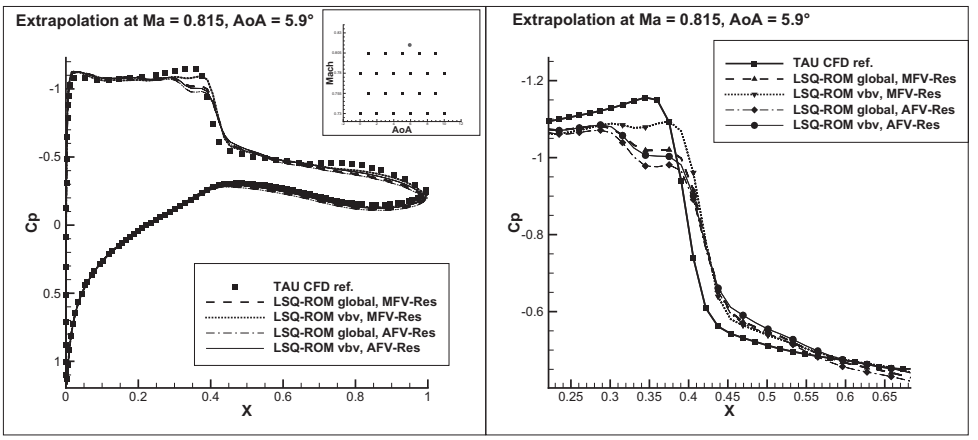

Figure 4. Comparison of the C_p-distributions for NACA 64A010 aerofoil approximated via global and variable-by-variable LSQ-ROM with the converged reference TAU CFD solution at the extrapolatory condition Ma = 0·815 and α = 5·9°. The abbreviation 'MVF-Res' indicates a solution obtained by considering only the mean flow variables when solving Equation (13). 'AVF-Res' indicates considering all flow variables, turbulence residuals included, when solving Equation (13). Right: detailed view of the shock region.

Table 1
Results for NACA 64A010 aerofoil at extrapolatory flow conditions .
(Ma = 0·815, α = 5·9°).

Procedure	CFD residual evaluations	CPU time	C_L	C_D
TPS	—	3s	0·6088 (0·14%)	0·0758 (–1·65%)
Global Kriging	—	3s	0·5972 (–1·77%)	0·0744 (–1·77%)
Var-by-var Kriging	—	3s	0·5856 (–3·65%)	0·0727 (–5·67%)
LSQ-ROM, MFV-Res, global	41	6·5s	0·6130 (0·84%)	0·0732 (–4·96%)
LSQ-ROM, MFV-Res, vbv	187	101s	0·6133 (0·88%)	0·0752 (–2·38%)
LSQ-ROM, AFV-Res, global	38	6·5s	0·6094 (0·25%)	0·0724 (–6·01%)
LSQ-ROM, AFV-Res, vbv	138	32s	0·6109 (0·48%)	0·0740 (–3·93%)
TAU CFD reference	2,137	400s	0·6079	0·0770

The abbreviation 'MVF-Res' indicates a solution obtained by considering only the mean flow variables, see Equation (4), when solving Equation (13). 'AVF-Res' indicates considering all flow variables, turbulence residuals included, when solving Equation (13).

feature a strong step at the shock location. The TPS solution has a second step slightly downstream of the shock. In addition, the Kriging solutions show severe oscillatory behaviour upstream of the shock. The various LSQ-ROM solutions displayed in Fig. 4 mitigate the step at the shock at the cost of predicting the shock location slightly further downstream and of a larger difference to the CFD reference towards the tail of the profile.

Table 1 compares the required number of full-order CFD residual evaluations, the CPU time as well as the lift and drag coefficients, C_L and C_D, for the various methods. Surprisingly, despite the rather poor predicted surface pressure distribution, the TPS solution features the lowest approximation error with respect to the integral values when compared to the TAU reference

https://doi.org/10.1017/S0001924000007491 Published online by Cambridge University Press

Table 2
Residual norms of the approximate solutions at extrapolatory flow conditions (Ma = 0·815, α = 5·9°) as listed in Table 1

Procedure	$\|\Omega^{-1}\text{res}(E)\|$	$\|\Omega^{-1}\text{res}(u_x)\|$	$\|\Omega^{-1}\text{res}(u_z)\|$	$\|\Omega^{-1}\text{res}(\rho)\|$	$\|\Omega^{-1}\text{res}(\nu)\|$	Σ
TPS	0·2872	0·1436	0·0333	0·0630	1·9716e–04	0·5273
Kriging, gl	0·5757	0·2841	0·0568	0·1170	1·9051e–04	1·0338
Kriging, vbv	1·7232	0·5200	0·0927	0·4064	2·0305e–04	2·7424
LSQ-ROM, MFV-Res, gl.	0·1469	0·0845	0·0248	0·0339	1·7783e–04	0·2903
LSQ-ROM, MFV-Res, vbv	0·0994	0·0574	0·0166	0·0190	4·3481e–04	0·1929
LSQ-ROM, AFV-Res, gl.	0·1559	0·0874	0·0279	0·0365	1·6253e–04	0·3078
LSQ-ROM, AFV-Res, vbv	0·1334	0·0776	0·0223	0·0247	1·3946e–04	0·2582
TAU CFD reference	7·6458e–05	8·1404e–05	1·9738e–05	3·9626e–05	1·3957e–04	3·6e–04

The abbreviation 'MVF-Res' indicates a solution obtained by considering only the mean flow variables, see Equation (4), when solving Equation (13). 'AVF-Res' indicates considering all flow vars, turbulence residuals included, when solving Equation (13).

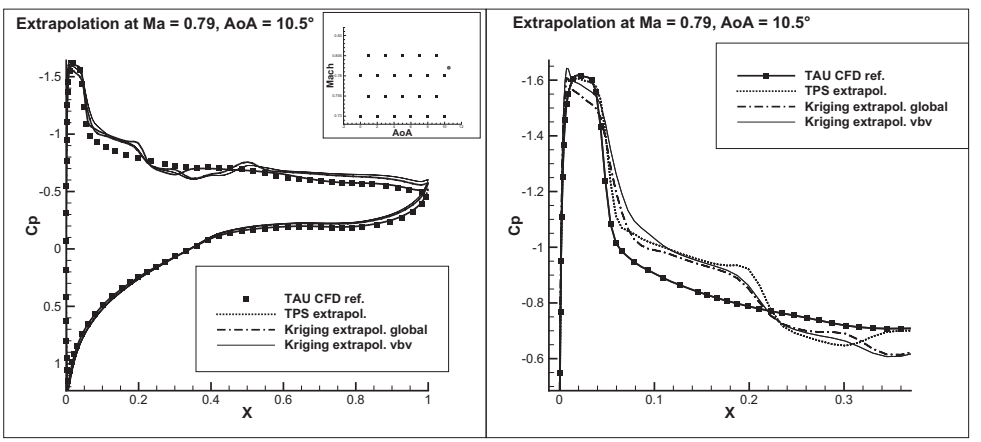

Figure 5. Comparison of the C_p-distributions for NACA 64A010 aerofoil approximated via TPS extrapolation and global and variable-by-variable Kriging extrapolation with the converged reference TAU CFD solution at Ma = 0·79, α = 10·5°. Right: detailed view of the shock region.

solution. This is partly explained by Corollary A.3, because TPS extrapolation combined with POD leads to the same result as scalar TPS extrapolation of the global coefficients without knowing the underlying pressure distributions.

The norms of the residuals of the various solutions are given in Table 2 for different flow variables. The norms are computed with respect to the discrete L_2 norm as stated in Equation (13). As expected from theory, all LSQ-ROM solutions feature significantly lower residuals than their extrapolation counterparts, with the variable-by-variable LSQ-ROM solutions showing the lowest objective function value in the L_2-sense. The variable-by-variable approach, however, comes at a significantly higher computational cost.

https://doi.org/10.1017/S0001924000007491 Published online by Cambridge University Press

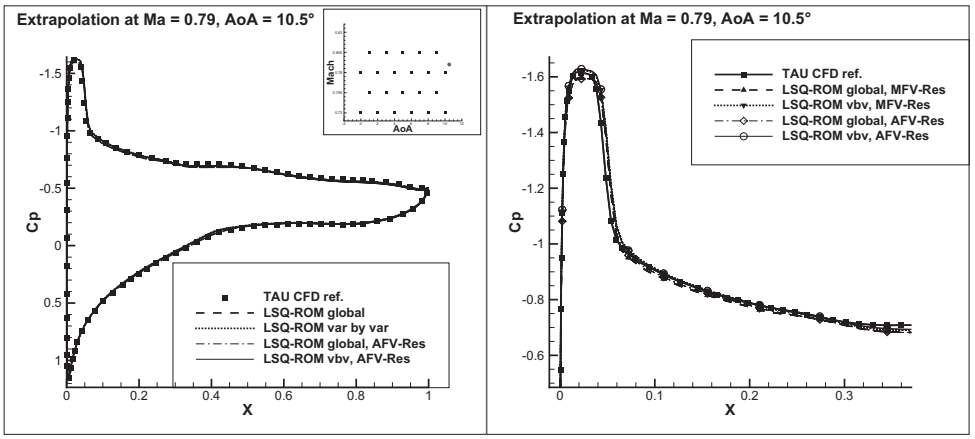

Figure 6. Comparison of the C_p-distributions for NACA 64A010 aerofoil approximated via global and variable-by-variable LSQ-ROM with the converged reference TAU CFD solution at the extrapolatory condition Ma = 0·79, α = 10·5°. The abbreviation 'MVF-Res' indicates a solution obtained by considering only the mean flow variables, see Equation (4), when solving Equation (13). 'AVF-Res' indicates considering all flow vars, turbulence residuals included, when solving Equation (13). Right: detailed view of the shock region.

Table 3
Results for NACA 64A010 aerofoil at extrapolatory flow conditions; Ma = 0·79, α = 10·5°

Procedure	CFD residual evaluations	CPU time	C_L	C_D
TPS	-	3s	0·7158 (1·97%)	0·15340 (1·02%)
Kriging global	-	3s	0·7205 (2·64%)	0·15950 (5·04%)
Kriging vbv	-	3s	0·7268 (3·53%)	0·16008 (5·42%)
LSQ-ROM, MFV-Res, global	49	7·7s	0·6870 (–2·14%)	0·14920 (–1·74%)
LSQ-ROM, MFV-Res, vbv	150	47s	0·6877 (–2·04%)	0·14766 (–2·76%)
LSQ-ROM, AFV-Res, global	48	7·9s	0·6841 (–2·55%)	0·14819 (–2·41%)
LSQ-ROM, AFV-Res, vbv	154	67s	0·6893 (–1·81%)	0·14733 (–2·97%)
TAU CFD ref.	3,927	703s	0·7020	0·15185

The abbreviation 'MVF-Res' indicates a solution obtained by considering only the mean flow variables, see Equation (4), when solving Equation (13). 'AVF-Res' indicates considering all flow vars, turbulence residuals included, when solving Equation (13).

3.1.2 Extrapolation at (Ma = 0·79, α = 10·5°)

Similar behaviour can be observed at the second trial point (Ma = 0·79, α = 10·5°). As displayed in Fig. 5, the POD-based extrapolation results again show a step near the shock and severe oscillatory behaviour while the corresponding LSQ-ROM results displayed in Fig. 6 match almost perfectly the CFD reference.

The corresponding aerodynamic coefficients, the required number of full-order CFD residual evaluations and the CPU time investments are shown in Table 4, while the residual norms are given in Table 3. Again, it is the TPS solution, which matches best the global aerodynamic coefficients, while the LSQ-ROM solutions feature by far the smallest residuals. From the aerodynamic point

https://doi.org/10.1017/S0001924000007491 Published online by Cambridge University Press

Table 4
Residual norms of the approximate solutions at extrapolatory flow conditions (Ma = 0·79, α = 10·5°) as listed in Table 3

Procedure	$\|\Omega^{-1}\mathrm{res}(E)\|$	$\|\Omega^{-1}\mathrm{res}(u_x)\|$	$\|\Omega^{-1}\mathrm{res}(u_z)\|$	$\|\Omega^{-1}\mathrm{res}(\rho)\|$	$\|\Omega^{-1}\mathrm{res}(\nu)\|$	Σ
TPS	0·4752	0·1874	0·0677	0·1126	5·6289e–04	0·8434
Kriging, gl	0·4352	0·1977	0·0876	0·1010	4.8847e–04	0·8221
Kriging, vbv	2·3316	0·6029	0·2623	0·6430	6·9841e–04	3·8406
LSQ-ROM, MFV-Res, gl.	0·0733	0·0374	0·0180	0·0170	4·3250e–04	0·1462
LSQ-ROM, MFV-Res, vbv	0·0560	0·0303	0·0134	0·0107	3·9965e–04	0·1108
LSQ-ROM, AFV-Res, gl.	0·0728	0·0338	0·0206	0·0164	3·8978e–04	0·1440
LSQ-ROM, AFV-Res, vbv	0·0613	0·0388	0·0173	0·0114	2·7121e–04	0·1291
TAU CFD reference	1·4419e–04	1·4487e–04	4·2095e–05	3·7710e–05	4·7118e–04	0·0008

of view, in both of the cases above, the LSQ-ROM approximations feature a much more physical surface pressure distribution than the approximations obtained via POD-based extrapolation. Considering the results in Tables 1, 2, 3 and 4 it can be deduced that the norm of the residuals is a more appropriate measure for judging the quality of the flow approximations than comparing global coefficients.

For such a small test case, it is understood that the computational time of the ROM methods is dominated by computational overhead, rendering a comparison of the actual ROM benefits questionable. Yet, it is important to note that the number of residual evaluations, which accrue for the LSQ-ROM results only, depends on the number of modes $\tilde{m}$! For cases with very large computational grids, the number of residual evaluations required to obtain a converged CFD solution may increase dramatically, while the number of residual evaluations that are due in the least-squares optimisation will essentially stay the same if the number of modes remains the same. This hypothesis is supported by the example presented in the following section, which will also be more telling in regard of computational savings.

3.2 Navier-Stokes LSQ-ROM for transonic flow around the NASA Common Research Model (NASA CRM)

In this section, we present a reduced-order model of the compressible Reynolds-averaged Navier-Stokes equations for the turbulent flow around the NASA common research model (NASA CRM[16]), which is representative of a wide-body commercial transport aircraft configuration. The six CFD snapshots used to construct the ROM were computed with the DLR RANS flow solver TAU[7-9] at a constant cruise Mach number of 0·85 and at angles-of-attack of α = 0·0°, 2·0°, 4·0°, 6·0°, 8·0°, 10·0°. The Reynolds number is fixed throughout at a value of 5 million. The unstructured computational grid used to compute the snapshots consists of 4,074,967 million grid points and is shown in part in Fig. 7. As explained in Remark 2.1, when using the Spalart-Allmaras one-equation turbulence model[17], the TAU solutions feature 7 flow variables resulting in a total dimension of the solution state vectors (and the global POD modes) of $n_t = vn = 7 \cdot 4{,}074{,}967 = 28{,}524{,}769$. Converged CFD snapshots and a reference CFD solution were computed on an HPC cluster in parallel, distributed on 24 domains (two nodes, 12 cores each). The LSQ-ROM optimisation procedure has been fully parallelised and was conducted on the same HPC cluster distributed to the same number of domains.

A global POD of the snapshot data gives an orthogonal representation, where the first five modes capture the complete information contained in the snapshots. Pursuing the variable-by-variable

https://doi.org/10.1017/S0001924000007491 Published online by Cambridge University Press

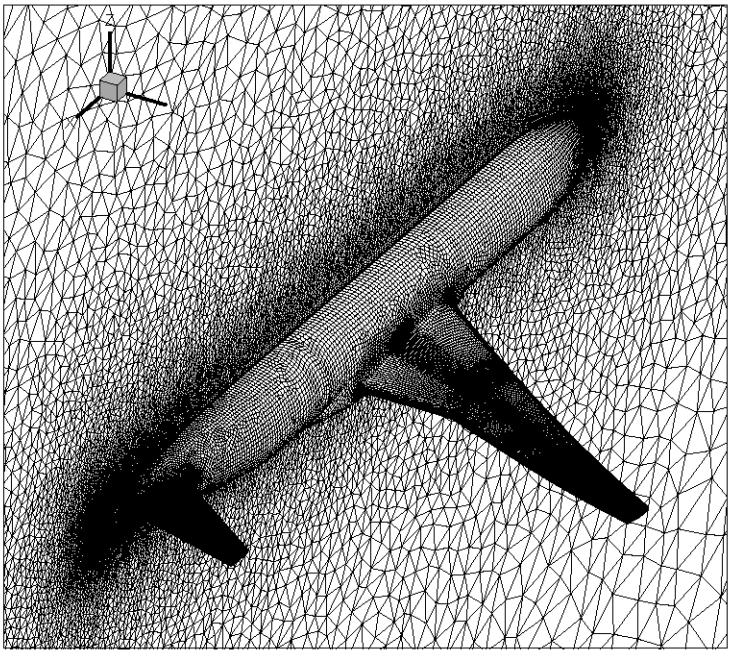

Figure 7. Computational grid for the NASA Common Research Model featuring ~ 4·1 mio. points in complete volume grid[24].

POD approach, we obtain POD sub-bases for density, x-velocity, y-velocity, pressure, the SA-viscosity and the eddy viscosity, each consisting of 5 POD modes that capture the complete relative information content, leading to a total of $7 \bullet 5 = 35$ mode vectors of size $n = 4{,}074{,}967$. Note that, as before, the mean flow vector is a constant vector that is not subject to any estimation/optimisation procedure.

Therefore, using global POD the initial flow problem of order $n_t = 28{,}524{,}769$ is reduced, in this case, to an order-5 optimisation problem (Equation (13)). When pursuing the variable-by-variable POD approach, the optimisation problem (Equation (13)) is of order 35.

As a trial point for the reduced-order methods, ($Ma = 0{\cdot}85$, $\alpha = 12{\cdot}0^{\circ}$) was chosen, i.e. a flow condition beyond the range of angles-of-attack of the snapshots set. The remaining free-stream conditions were kept constant throughout. Such kind of extrapolatory predictions are required for efficiently computing aerodynamic polars, see Ref. 23. Notice that a step of two degrees beyond the range covered by the snapshots is comparably large and is chosen here only to show the capability of the method. In general one cannot expect the ROM to behave well at conditions for which no comparable snapshot information has been provided and therefore, in realistic applications, such extreme cases of extrapolation should be avoided. Moreover, with separated flow present, this is a very challenging test case for any reduced-order approach.

At the flow condition of ($Ma = 0{\cdot}85$, $\alpha = 12{\cdot}0^{\circ}$), the approximate solutions obtained by TPS extrapolation and global Kriging feature non-physical values. Thus, they are not even fit for use as initial solutions to the LSQ-ROM procedure! Therefore, the LSQ-ROM approach was initialised with the POD coefficients corresponding to the CFD snapshot at $\alpha = 10{\cdot}0^{\circ}$. Knowing the index of this snapshot, its POD coefficients can be read from Equation (12). Kriging based on variable-by-variable POD, on the other hand, leads to an admissible result. However, in the case of the

https://doi.org/10.1017/S0001924000007491 Published online by Cambridge University Press

Table 5
Results for the NASA CRM at extrapolatory flow conditions (Ma = 0·85, α = 12±)

Procedure CFD	res. evals.	CPU time	C_L	C_D
TPS	—	20s	NaN	NaN
Kriging gl.	—	20s	NaN	NaN
Kriging vbv	—	20s	0·9040 (2·61%)	0·2128 (2·47%)
LSQ-ROM (1)	18	59s	0·8932 (1·39%)	0·2190 (0·36%)
LSQ-ROM (2)	31	72s	0·8702 (–1·22%)	0·2114 (–3·13%)
TAU CFD ref.	10,000	8,500s	0·8809	0·2182

Legend: LSQ-ROM (1): solution obtained via global POD when minimising Equation (13) with respect to the mean flow variables only started from the coefficients of the CFD snapshot at α = 10°; LSQ-ROM (2): solution obtained via global POD when minimising Equation (13) including the turbulence residuals, started from the coefficients of the CFD snapshot at α = 10°. Global Kriging and thin-plate-spline extrapolation result in non-physical solutions.

Table 6
Residual norms of the approximate solutions at extrapolatory flow conditions (Ma = 0·85, α = 12°) as listed in Table 5

Procedure	$\|\Omega^{-1}\mathrm{res}(E)\|$	$\|\Omega^{-1}\mathrm{res}(u_x)\|$	$\|\Omega^{-1}\mathrm{res}(u_y)\|$	$\|\Omega^{-1}\mathrm{res}(u_z)\|$	$\|\Omega^{-1}\mathrm{res}(\rho)\|$	$\|\Omega^{-1}\mathrm{res}(\nu)\|$	Σ
TPS	NaN	NaN	NaN	NaN	NaN	NaN	NaN
Kriging, gl	NaN	NaN	NaN	NaN	NaN	NaN	NaN
Kriging, vbv	2·14e–03	4·15e–04	1·79e–04	1·62e–04	5·03e–04	7·86e–07	3·22e–03
LSQ-ROM (1)	2·57e–04	1·16e–04	3·74e–05	7·79e–05	5·42e–05	5·45e–07	5·06e–04
LSQ-ROM (2)	4·44e–04	1·52e–04	4·09e–05	2·13e–04	1·03e–04	3·10e–07	9·12e–04
TAU CFD reference	1·77e–08	7·41e–09	5·79e–09	1·90e–09	4·51e–08	3·17e–07	3·89e–07
TAU CFD at α = 10°	6·95e–04	2·20e–04	5·78e–05	3·62e–04	1·63e–04	2·14e–07	1·44e–03

Since the LSQ-ROM solutions (1) and (2) were obtained by starting the optimisation procedure Equation (13) from the POD coefficients associated to the TAU snapshot at α = 10°, the residual norms of this precise solution w.r.t. the boundary condition α = 12° are also given. Note that the Kriging solution features a residual even larger than the solution at α = 10°.

variable-by-variable LSQ-ROM the optimiser got stuck in the initial solution when initialised with both the POD coefficient of the CFD snapshot at α = 10·0° and those predicted by Kriging extrapolation at α = 12·0°, thus detecting a local minimum. This was the case when optimising Equation (13) with respect to the mean flow variables only, as well as when optimising Equation (13) with respect to the complete set of residual variables. As a consequence, no variable by- variable LSQ-ROM results are included in Tables 5 and 6. Table 5 compares the number of full-order CFD residual evaluations that were required to solve Equation (13), the computational time and the integrated lift and drag coefficients, C_L and C_D, including relative errors with respect to the CFD reference solution for the various methods.

The LSQ-ROM solution obtained via global POD when minimising Equation (13) with respect to the mean flow variables only features the smallest relative errors as well as the smallest residual. In regard of the absolute computational time, an acceleration by a factor of 144 is obtained when compared to a full-order CFD simulation. The associated surface C_p-distribution is displayed in Fig. 8. Figures 9, 10 compare the associated C_p-distributions at various wing section cuts.

Although exhibiting differences to the reference solution downstream of the leading-edge suction peak, it is remarkable that the LSQ-ROM solution resolves the downstream pressure distribution with considerable accuracy, while the extrapolated solution again features a step-like behavior. This is in line with the observations obtained for the aerofoil in Section 3.1.

https://doi.org/10.1017/S0001924000007491 Published online by Cambridge University Press

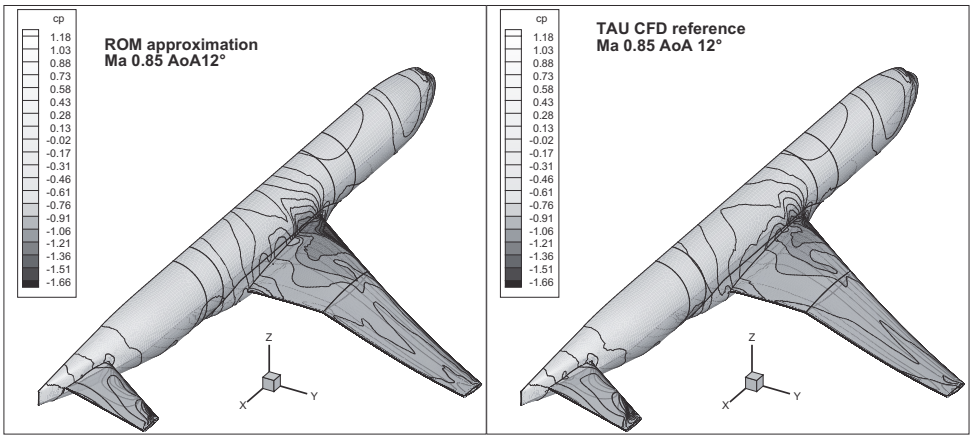

Figure 8. Comparison of the C_p-distributions approximated via the global POD-based least-squares ROM with the converged reference TAU CFD solution in the transonic flow regime at α = 12·0°.

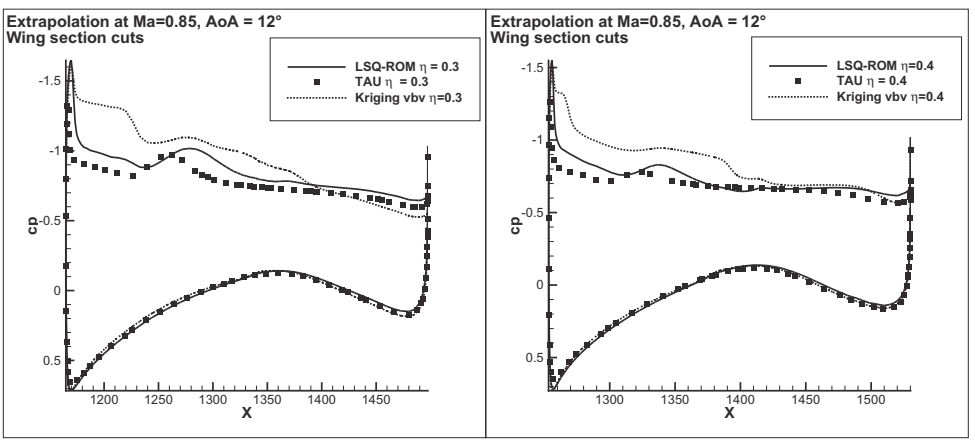

Figure 9. Comparison of the C_p-distributions for the NASA CRM approximated via the global PODbased least-squares ROM and variable-by-variable Kriging extrapolation with the converged reference TAU CFD solution in the transonic flow regime at extrapolatory conditions Ma = 0·85, α = 12·0°. Wing section cuts at a wing span of 30% (left) and 40% (right).

4.0 CONCLUSIONS

A POD-based ROM of the governing equations of fluid dynamics was presented and applied to steady aerodynamics problems. Using this approach, the problem of solving the governing equations was replaced by a low-order optimisation problem. Global POD as opposed to variable-by-variable POD was discussed.

As test cases, a two-parameter ROM for the NACA 64A010 aerofoil as well as a one-parameter ROM for the NASA Common Research Model (CRM) were presented, the latter one being representative of a commercial wide-body passenger aircraft. In both cases, fully turbulent compressible transonic flows were considered at challenging extrapolatory conditions. For the NASA CRM example even flow separation occurred.

https://doi.org/10.1017/S0001924000007491 Published online by Cambridge University Press

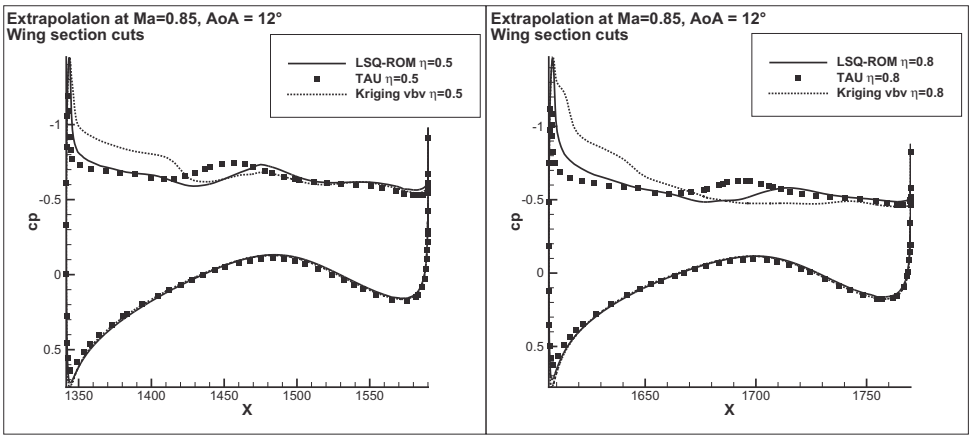

Figure 10. Comparison of the C_p-distributions approximated via the global POD-based least-squares ROM and variable-by-variable Kriging extrapolation with the converged reference TAU CFD solution in the transonic flow regime at extrapolatory conditions Ma = 0·85, α = 12·0°. Wing section cuts at a wing span of 50% (left) and 80% (right).

Based on the examples investigated in this work, we conclude that the variable-by-variable POD approach suffers from a lack of robustness and a significantly higher computational costs, while the theoretical benefits do not pay off considerably when comparing the global and the variable-by-variable solutions. Moreover, it has been proved that when following the POD-based interpolation approach applying radial basis functions, global and variable-by-variable interpolation of POD coefficients lead to the same result.

In terms of computation time, a substantial speed-up (two orders of magnitude for the NASA CRM) was observed when compared to the CFD reference computation.

In regard of the approximation accuracy, we observed the following: Without any exception, the flow approximations obtained via the POD-based extrapolation methods all showed a step function-like behavior in the surface pressure distribution at the corresponding shock location. In contrast, the LSQROM approximations showed a sharp shock or at least mitigated the step at the shock and thus featured a much more physical overall pressure distribution. This corresponds to a significantly lower CFD residual in the L_2 -norm when comparing the LSQ-ROM solutions to the POD-extrapolated solutions.

We conclude that considering CFD residuals is a much more appropriate way of judging distributed data than relying on errors in global coefficients.

When it comes to global integral coefficients, however, no superiority of the LSQ-ROM methods to its competitors could be observed. In this regard, the RBF interpolation using TPS correlation matches best the CFD reference, despite its unphysical pressure distribution. It was proposed that the RBF approach leads to consistent results when the dependence between distributed data and global coefficients is linear. In other words, the approximation quality of the RBF solutions in terms of the aerodynamic coefficients is the same as when the global coefficients themselves are considered as sample values, without even knowing the corresponding pressure distribution.

When extrapolating the aerodynamics of the NASA CRM, global POD combined with Kriging and TPS interpolation of the POD coefficients actually failed in providing a physically admissible solution, rendering the LSQ-ROM method the only viable approach next to variable-by-variable POD combined with Kriging.

https://doi.org/10.1017/S0001924000007491 Published online by Cambridge University Press

While not demonstrated in this work, it is understood that the LSQ-ROM approach is also applicable for the (less challenging) task of interpolation. In this regard, the reader is referred to e.g. Ref. 19.

A word of caution: The LSQ-ROM approach is limited to the computational space spanned by the input snapshot solutions (this being the whole idea about reduced order modeling). In other words, flow phenomena not contained in this space cannot be predicted by no matter what sophisticated method. As a consequence, the snapshot sampling is a crucial step in constructing the ROM.

ACKNOWLEDGMENTS

This research was sponsored in part by the European Regional Development Fund, Economic Development Fund of the Federal German State of Lower Saxony, contract/grant number: W3-80026826, and the German Federal Ministry of Economics and Technology (BMWi).

REFERENCES

1. KLENNER, J., BECKER, K., CROSS, M. and KROLL, N. Future simulation concept, 2007, First CEAS Conference, 2007-09-10, Egmond and Zee, Berlin, Germany.
2. TINOCO, E.N., BOGUE, D.R., KAO, T.J., YU, N.J., LI, P. and BALL, D.N. Progress toward CFD for full flight envelope, *Aeronaut J*, October 2005, **109**, (1100), pp 451–460.
3. SALAS, M.D. Digital flight: The last CFD grand challenge, *J Scientific Computing*, 2006, **28**, (213), pp 479–505.
4. ZIMMERMANN, R. and GÖRTZ, S. Non-linear reduced order models for steady aerodynamics, *Procedia Computer Science,* 2010, **1**, (1), pp 165–174.
5. ZIMMERMANN, R. and GÖRTZ, S. Non-linear POD-based reduced order models for steady turbulent aerodynamics, 2010, RAeS 2010 Conference Applied Aerodynamics: Capabilities and Future Requirements, Bristol, UK.
6. LEGRESLEY, P. A. and ALONSO, J.J. Investigation of non-linear projection for POD-based reduced order models for aerodynamics, 2001, AIAA Paper, number 2001-0926.
7. GERHOLD, T., FRIEDRICH, O., EVANS, J. and GALLE, M. Calculation of complex three-dimensional configurations employing the dlr-tau-code, 1997, AIAA-Paper number 97-0167.
8. GALLE, M., GERHOLD, T. and EVANS, J. Parallel computation of turbulent flows around complex geometries on hybrid grids with the dlr-tau code, 1999, 11th Parallel CFD Conference, 23-26 May 1999, ECER, A. and R., E.D., (Eds).
9. SCHWAMBORN, D., GERHOLD, T. and HEINRICH, R. The dlr tau-code: recent applications in research and industry, 2006, Technical Report, European Conference on Computational Fluid Dynamics, ECCOMAS CFD 2006, Egmond and Zee, The Netherlands.
10. FORRESTER, A.I.J., SOBESTER, A. and KEANE, A.J. *Engineering Design via Surrogate Modelling: A Practical Guide*, 2008, John Wiley & Sons, UK.
11. CHATURANTABUT, S. and SORENSEN, D. Discrete empirical interpolation for nonlinear model reduction, 2009, Technical Report TR09-05, Rice University, Houston, TX, USA.
12. ASTRID, P., WEILAND, S., WILCOX, K. and BACKX, T. Missing points estimation in models described by proper orthogonal decomposition, *IEEE Transactions on Automatic Control*, 2008, **53**, (10), pp 2237-2251.
13. BUI-THANH, T., DAMADORAN, M. and WILLCOX, K. Proper orthogonal decomposition extensions for parametric applications in transonic aerodynamics, 2003, 2003-4213 AIAA, 21th AIAA Applied Aerodynamics Conference, Orlando, FL, USA.
14. SACKS, J., WELCH, W.J., MITCHELL, T.J. and WYNN, H.P. Design and analysis of computer experiments, *Statistical Science*, 1989, **4**.
15. HAN, Z.H., GÖRTZ, S. and ZIMMERMANN, R. On improving efficiency and accuracy of variable-fidelity surrogate modeling in aero-data for loads context, 2009, CEAS 2009 European Air and Space conference, Manchester, UK.

16. VASSBERG, J.C., DEHAAN, M.A., RIVERS, S.M., and A., W.R. Development of a common research model for applied CFD validation studies, 2008, AIAA 2008-6919, 26th AIAA Applied Aerodynamics Conference, Hawaii, HI, USA.
17. BLAZEK, J. *Computational Fluid Dynamics: Principles and Applications*, 2001, First edition, Elsevier, Amsterdam – London – New York – Oxford – Paris – Shannon – Tokyo.
18. PINNAU, R. Model reduction via proper orthogonal decomposition, 2008, *Model Order Reduction: Theory, Research Aspects and Applications*, SCHILDERS, W.H.A., VAN DER VORST, H.A. and ROMMES, J. (Eds), volume 13 of Springer Series *Mathematics in Industry*, 95–109. Springer.
19. ZIMMERMANN, R. Towards best-practice guidelines for POD-based reduced order modeling of transonic flows, 2011, EUROGEN 2011, POLONI, C., QUAGLIARELLA, D., PÉRIAUX, J., GAUGER, N. and GIANNAKOGLOU, K. (Eds), CIRA — Italian Aerospace Research Centre, Capua, Italy.
20. HOLMES, P., LUMLEY, J., and BERKOOZ, G. *Turbulence, Coherent Structures, Dynamical Systems and Symmetry,* 1996, Cambridge University Press, Cambridge, UK.
21. SANTNER, T.J., WILLIAMS, B.J. and NOTZ, W.I. *The Design and Analysis of Computer Experiments*, 2003, Springer, New York, Berlin, Heidelberg.
22. MADSEN, K., NIELSEN, H.B. and TINGLEFF, O. *Methods for Non-linear Least Squares Problems, IMM Informatics and Mathematical Modelling*, April 2004, Second edition, Technical University of Denmark.
23. MIFSUD, M., ZIMMERMANN, R., SIPPLI, J. and GÖRTZ, S. A POD-based reduced order modeling approach for the efficient computation of high-lift aerodynamics, 2011, EUROGEN 2011, POLONI, C., QUAGLIARELLA, D., PÉRIAUX, J., GAUGER, N. and GIANNAKOGLOU, K. (Eds), (CIRA —Italian Aerospace Research Centre, Capua, Italy.
24. CRIPPA, S. Improvement of unstructured computational fluid dynamics simulations through novel mesh generation methodologies, *J Aircr*, 2011, **48**, (3), pp 1036-1044.

APPENDIX

A1 PROOFS OF THE STATEMENTS FROM SECTION 2.3

A1.1 Theorem A.1 (a fundamental remark on POD-based interpolation via RBFs)

Entry-by-entry interpolation of the snapshot vectors and interpolation of the basis coefficients when considering the snapshot vectors themselves as a basis lead to the same results when applying radial basis function interpolation. Provided that the maximum number of POD modes $\tilde{m} = m - 1$ is retained in the POD basis, then interpolation of POD coefficients with respect to global POD modes and interpolation of POD coefficients with respect to variable-by-variable POD modes again lead to the same result. Moreover, the RBF interpolation result is invariant under changes of coordinates.

A1.1.1 Proof

Let $\{p^1, ..., p^m\} \subset \mathbb{R}^d$ be a set of sample locations with $\mathbf{f}^T = (f_1, .., f_m)^T = (f(p^1), ..., f(p^m))^T \in \mathbb{R}^m$ being the corresponding vector of sample values. At an untried location p^*, the radial basis function interpolant takes the value

$$\hat{f}(p^*) = \mathrm{f}^T \Psi^{-1} \psi(p^*), \qquad \ldots (A.1)$$

https://doi.org/10.1017/S0001924000007491 Published online by Cambridge University Press

where $\psi(p^*) = \psi(\| p^* - p^1 \|), ..., \psi(\| p^* - p^1 \|)$ is the vector of radial distances of the test location to the sample locations, $\Psi = \psi(\| p^i - p^j \|)_{i,j} \in \mathbb{R}^{m \times m}$ is the so-called Gram matrix and $\psi : r \mapsto \psi(r)$ is the radial basis function of choice.

Given a set of data vectors

$$\mathbf{W}(p^1) = \begin{pmatrix} W_1(p^1) \\ \vdots \\ W_n(p^1) \end{pmatrix}, ..., \mathbf{W}(p^m) = \begin{pmatrix} W_1(p^m) \\ \vdots \\ W_n(p^m) \end{pmatrix} \in \mathbb{R}^n \quad \ldots (A2)$$

and let $\mathbf{Y} = (\mathbf{W}(p^1), ..., \mathbf{W}(p^m) \in \mathbb{R}^{n \times m}$.

Entry-by-entry interpolation via RBFs leads to

$$\hat{W}_i(p^*) = \left(W_i(p^1), ..., W_i(p^m)\right) \Psi^{-1} \boldsymbol{\psi}(p^*) \quad \ldots (A3)$$

for $i = 1, ..., n$. It follows that

$$\begin{pmatrix} \hat{W}_1(p^*) \\ \vdots \\ \hat{W}_n(p^*) \end{pmatrix} = \begin{pmatrix} \left(W_1(p^1), ..., W_1(p^m)\right) \Psi^{-1} \boldsymbol{\psi}(p^*) \\ \vdots \\ \left(W_n(p^1), ..., W_n(p^m)\right) \Psi^{-1} \boldsymbol{\psi}(p^*) \end{pmatrix} = \mathbf{Y} \Psi^{-1} \boldsymbol{\psi}(p^*) \quad \ldots (A4)$$

$$= \sum_{j=1}^{m} \left(\Psi^{-1} \boldsymbol{\psi}(p^*)\right)_j \mathbf{W}(p^j) = \sum_{j=1}^{m} \left(e_j^T \Psi^{-1} \boldsymbol{\psi}(p^*)\right) \mathbf{W}(p^j). \quad \ldots (A5)$$

Notice that the co-ordinate vector of $\mathbf{W}(p^j)$ with respect to the basis $\{\mathbf{W}(p^1), ..., \mathbf{W}(p^m)\}$ is given by $e_j = (0, ..., 1, ...0)^T$. Therefore, the coefficient $x_j = (e_j^T \Psi^{-1} \psi(p^*)$ in Equation (A5) is exactly the result of the RBF interpolant at p^* for the vector of sample values e_j !

The remaining claims come as a straight forward consequence, when replacing $\mathbf{Y}$ by its global or var-by-var POD representation in Equation (A4).

A1.2 Theorem A.2

Let $\mathbf{W}^1, ..., \mathbf{W}^m \in \mathbb{R}^n$ be vectors and let $L : \mathbb{R}^n \to \mathbb{R}$ be linear, i.e. $L(\mathbf{W}^i + \lambda \mathbf{W}^j) = L(\mathbf{W}^i) + \lambda L(\mathbf{W}^j)$ for any number $\lambda \in \mathbb{R}$. Let $\tilde{\mathbf{W}}^*$ be the resulting vector when performing RBF interpolation for the set of sample vectors $\mathbf{W}^1, ..., \mathbf{W}^m \in \mathbb{R}^n$ at a location p^* and let l^* be the result when performing RBF interpolation on the set of scalar sample values $L(\mathbf{W}^1), ..., L(\mathbf{W}^m)$. Then $l^* = L(\tilde{\mathbf{W}}^*)$.

A1.2.2 Proof

Keeping the notations for the RBF correlation vector and matrix as introduced above, let $\mathbb{R}^m \ni q^* := \Psi^{-1} \psi(p^*)$. RBF interpolation of the vector data at an untried condition p^* leads to $\hat{\mathbf{W}}^* = (\mathbf{W}^1, ..., \mathbf{W}^m)\mathbf{q}^* = \sum_{i=1}^{m} q_i^* \mathbf{W}^i$, see Equation (A4). RBF interpolation of the scalar values gives $l^* = (L(\mathbf{W}^1), ..., L(\mathbf{W}^m))\, q^*$, see Equation (A1). On the other hand we have;

$$L(\hat{\mathbf{W}}^*) = L\left(\sum_{i=1}^{m} q_i^* \mathbf{W}^i\right) = \sum_{i=1}^{m} q_i^* L(\mathbf{W}^i) = \left(L(\mathbf{W}^1), ..., L(\mathbf{W}^m)\right) \mathbf{q}^* = l^*. \quad \ldots (A6)$$

https://doi.org/10.1017/S0001924000007491 Published online by Cambridge University Press

A1.3 Corollary A.3 (consistency of distributed and integrated RBF interpolation of aerodynamics)

Performing RBF interpolation on field data and subsequently computing the corresponding lift, drag and moment coefficients leads to exactly the same result as performing scalar RBF interpolation on the integrated coefficients only without knowing any surface distribution.

A1.3.1 Proof

Via integration, the global aerodynamic lift, drag and moment coefficients C_L, C_D, C_{Mx}, C_{My}, C_{Mz} depend linear on the surface pressure, so that Equation (A4) applies.

https://doi.org/10.1017/S0001924000007491 Published online by Cambridge University Press